

## SHORT COMMUNICATIONS

### FINITE PLANE STRAIN DEFORMATIONS OF RUBBERLIKE MATERIALS

R. C. BATRA

*Department of Engineering Mechanics, University of Missouri-Rolla, Rolla, Mo., U.S.A.*

#### SUMMARY

A finite element program capable of analysing finite plane strain deformations of incompressible rubberlike (Mooney-Rivlin) materials has been developed. Two problems, namely a long wall loaded uniformly in two directions and a thick-wall cylindrical pressure vessel loaded internally, have been solved. The computed values of displacements, strains, stresses and hydrostatic pressure agree very closely with their values obtained analytically.

#### INTRODUCTION

A general purpose finite element program, NONSAP, capable of analysing linear and nonlinear, static and dynamic problems for elastic and elastic-plastic materials, has been developed by Bathe *et al.*<sup>1,2</sup> However, the capability to solve finite plane strain problems for incompressible elastic materials has not yet been incorporated into this program.

In the finite element formulation of finite plane strain problems for rubberlike materials, Scharnhorst and Pian<sup>3</sup> have used a Reissner-type variational principle and Oden<sup>4</sup> has employed the principle of stationary potential energy. The problem of the inflation of a thick-wall cylindrical pressure vessel made of a homogeneous Mooney-Rivlin material has been solved by Scharnhorst and Pian<sup>3</sup> and by Oden and Key<sup>5</sup> by employing the two different variational principles.

Our motive is to develop a finite element program capable of solving static finite plane strain problem. for incompressible elastic materials involving complex geometries and loading conditions. We follow Oden<sup>4</sup> and use the principle of stationary potential energy. We solve two problems for Mooney-Rivlin materials using this program and compare computed results with those obtained from their analytical solutions.

For the thick-wall pressure vessel problem, as is done in Reference 3, we use a 4-node plane strain isoparametric quadrilateral element with  $2 \times 2$  Gaussian integration rule to evaluate the integrals for the stiffness matrix. Comparison is made of the results obtained with those of Scharnhorst and Pian<sup>3</sup> and also of Oden and Key<sup>5</sup> who used axisymmetric formulation and constant strain triangular elements.

We note that for plane strain deformations of homogeneous Mooney-Rivlin materials, the values of displacements, strains and in-plane stresses for a given load distribution depend upon the two material constants only through their sum. Different choices of the values of the two constants with their sum being the same do result in different distributions of the hydrostatic pressure and the normal stress on the plane of deformation.

## FORMULATION OF THE PROBLEM

In this section we introduce the notation and give a summary of the equations used. Details of deriving these equations are given in References 3 and 4. We use fixed rectangular Cartesian co-ordinate axes to describe the position  $\mathbf{X}$  of a material particle in the reference configuration and its position  $\mathbf{x}$  in the present configuration. Therefore  $\mathbf{u} = (\mathbf{x} - \mathbf{X})$  gives the displacement of the material particle that occupied place  $\mathbf{X}$  in the reference configuration. The deformation gradient  $\mathbf{F}$ , the right Cauchy–Green tensor  $\mathbf{C}$  and the Green–Lagrange strain tensor  $\mathbf{E}$  are defined as

$$F_{ij} = \frac{\partial x_i}{\partial X_j} \equiv x_{i,j}, \quad C_{ij} = F_{ki}F_{kj}, \quad 2E_{ij} = C_{ij} - \delta_{ij}. \quad (1)$$

Throughout this paper we use the summation convention and in (1),  $\delta_{ij}$  is the Kronecker delta. The strain energy density  $W$  for isotropic elastic materials depends upon the strain tensor only through its principal invariants  $I_1$ ,  $I_2$  and  $I_3$ . For Mooney–Rivlin materials  $W$  is given by

$$W = C_1(I_1 - 3) + C_2(I_2 - 3), \quad I_1 = C_{ii}, \quad I_2 = I_3^{-1}(C^{-1})_{ii}, \quad I_3 = \det \mathbf{C} = 1. \quad (2)$$

Here  $C_1$  and  $C_2$  are material constants and for bodies homogeneous in the reference configuration, these assume the same values for each material point of the body.

Let the region occupied by the body in the reference configuration be subdivided into a finite number of subregions called elements. The principle of stationary potential energy states that within each element and hence for the entire body, the potential energy

$$P = \int_V \left( W + \frac{p}{2}(I_3 - 1) \right) dV - \int_A f_i u_i dA - \int_V \rho_0 g_i u_i dV \quad (3)$$

takes an extremum value [Reference 6, p. 253] for all admissible displacement fields that satisfy the displacement boundary condition. In (3),  $\mathbf{f}$  is the surface traction acting on a unit area in the reference configuration,  $\mathbf{g}$  is the body force per unit mass,  $\rho_0$  is the mass density and all the integrations are over regions in the reference configuration.  $\delta P = 0$  with  $W$  given by (2) gives

$$\int_V S_{ij} \delta E_{ij} dV = \int_A f_i \delta u_i dA + \int_V \rho_0 g_i \delta u_i dV, \quad (4)$$

$$\int_V \delta p (I_3 - 1) dV = 0,$$

in which

$$\mathbf{S} = p\mathbf{C}^{-1} + 2C_1\mathbf{1} + 2C_2(I_1\mathbf{1} - \mathbf{C}) \quad (5)$$

is the second Piola–Kirchhoff stress tensor. It is related to the Cauchy stress tensor  $\mathbf{T}$  by  $\mathbf{T} = (\mathbf{F}\mathbf{S}\mathbf{F}^T)/\det \mathbf{F}$ .

We assume that the given load is applied in  $M$ , not necessarily equal, increments and denote the incremental change in the value of say  $\mathbf{u}$  caused by the  $(N+1)$ st load increment by  $\Delta \mathbf{u}$ . That is

$$\mathbf{u}^{N+1} = \mathbf{u}^N + \Delta \mathbf{u}, \quad \mathbf{E}^{N+1} = \mathbf{E}^N + \Delta \mathbf{E}, \text{ etc.} \quad (6)$$

The relation between  $\Delta \mathbf{E}$  and  $\Delta \mathbf{u}$  obtained from equation (1) is

$$\Delta E_{ij} = \Delta e_{ij} + \Delta \eta_{ij}, \quad \Delta \eta_{ij} = \frac{1}{2} \Delta u_{k,i} \Delta u_{k,j}, \quad (7)$$

$$\Delta e_{ij} = \frac{1}{2} (\Delta u_{i,j} + \Delta u_{j,i} + u_{k,i}^N \Delta u_{k,j} + u_{k,j}^N \Delta u_{k,i}).$$

We note that  $\Delta I_3 = 2C_{ij}^{-1} \Delta E_{ij}$ . The relation between  $\Delta \mathbf{S}$ ,  $\Delta \mathbf{E}$  and  $\Delta p$  is given in Reference 3.

Setting  $\delta E_{ij} = \delta \Delta E_{ij}$ ,  $\delta u_i = \delta \Delta u_i$  and  $\delta p = \delta \Delta p$  in (4) we obtain

$$\int_V (S_{ij}^N + \Delta S_{ij}) \delta \Delta E_{ij} dV = \int_V \rho_0 g_i^{N+1} \delta \Delta u_i dV + \int_A f_i^{N+1} \delta \Delta u_i dA, \quad (8)$$

$$\equiv R^{N+1}.$$

$$\int_V \delta \Delta p ((C_{ij}^N)^{-1} \Delta E_{ij}) dV = -\frac{1}{2} \int_V \delta \Delta p (I_3^N - 1) dV. \quad (9)$$

We now make the assumption that the increment in the load is small so that

$$\Delta S_{ij} \delta \Delta E_{ij} \approx \Delta S_{ij} \delta \Delta e_{ij}, \quad (C_{ij}^N)^{-1} \Delta E_{ij} \approx (C_{ij}^N)^{-1} \Delta e_{ij},$$

$$\Delta S_{ij} \approx \frac{\partial S_{ij}}{\partial E_{kl}} \Delta e_{kl} + \frac{\partial S_{ij}}{\partial p} \Delta p = \frac{\partial S_{ij}}{\partial E_{kl}} \Delta e_{kl} + (C^{-1})_{ij} \Delta p.$$

Hence an approximation to equations (9) and (10) is

$$\int_V \Delta S_{ij} \delta \Delta e_{ij} dV + \int_V S_{ij}^N \delta \Delta \eta_{ij} dV \approx R^{N+1} - \int_V S_{ij}^N \delta \Delta e_{ij} dV,$$

$$\int_V \delta \Delta p (C_{ij}^N)^{-1} \Delta e_{ij} dV \approx -\frac{1}{2} \int_V \delta \Delta p (I_3^N - 1) dV.$$

If an analytical solution of a problem is known, then one can successively reduce the size of the load increment until a solution of equations (11) and (12) matches well with the analytical solution. This may require, depending upon the problem being solved, very large number of load steps. One can use equilibrium iterations,<sup>2,7</sup> i.e. iterations within a load step, to ensure that equations (11) and (12) are solved within a pre-specified error.

## COMPUTATION AND DISCUSSION OF RESULTS

A finite element program based on equations (11) and (12) and employing 4-node isoparametric quadrilateral elements with  $2 \times 2$  Gaussian integration rule has been written. The hydrostatic pressure  $p$  is assumed to be constant within an element. The body force  $g$  is taken to be zero. Even though for an assumed displacement field within a quadrilateral element, one can calculate consistent nodal loads, we have chosen to use lumped nodal loads since it is simpler to do so. If the applied load is dead, i.e. its magnitude and direction do not change during the deformation, then the equivalent nodal loads can be computed in the reference configuration. For distributed applied loads or for deformation dependent loads, one needs to compute nodal loads after each increment in the load. A distributed load on the boundary can be resolved into a pressure load and a tangential load. Let the pressure and the tangential load per unit length be denoted by  $\hat{p}$  and  $\hat{t}$ , respectively. Consider the line element between two nodes  $a$  and  $b$  on the bounding surface (see Figure 1). The total force  $f$  acting on the line element  $ab$  is given by

$$f_i = \hat{t}(x_i^b - x_i^a) - \hat{p} \varepsilon_{3ij} (x_j^b - x_j^a).$$

Therefore,

$$f_i^a = f_i^b = \frac{1}{2} [\hat{t}(x_i^b - x_i^a) - \hat{p} \varepsilon_{3ij} (x_j^b - x_j^a)]. \quad (13)$$

Here  $\varepsilon_{ijk}$  is the permutation symbol and it takes on values 1 or  $-1$  accordingly as  $i, j, k$  form an even or an odd permutation of 1, 2, and 3 and is zero otherwise. Since, after each increment in

load, the final positions of the nodes  $a$  and  $b$  are known, the nodes for the next load increment can be calculated based upon their positions computed after the immediately preceding load increment. Such an approach has also been suggested by Oden and Key.<sup>5</sup>

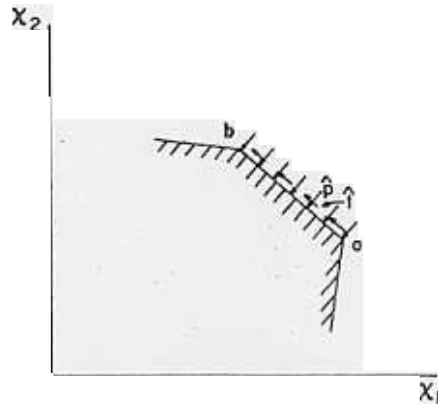


Figure 1. Distributed loading at the boundary

Below we discuss results for two sample problems. To ascertain the effect of the dissatisfaction of the incompressibility after the  $N$ th load step as given by the right-hand side of  $(12)_2$ , we also computed results with the right-hand side of  $(12)_2$  set equal to zero and found rather insignificant differences between the two sets of results. The results presented below are for the case when the right-hand side of  $(12)_2$  is taken to be zero.

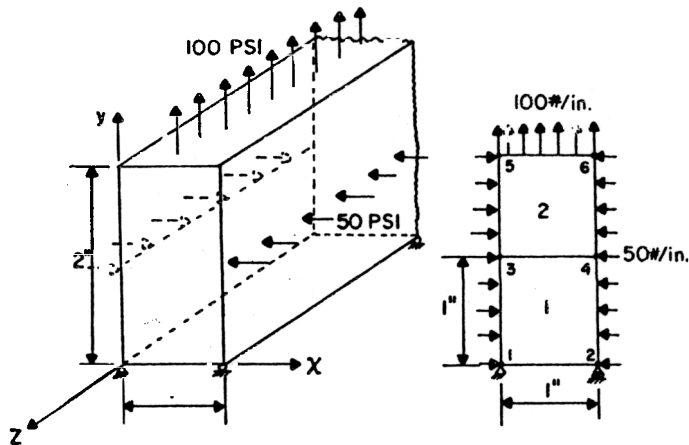


Figure 2. Biaxially loaded uniform wall

As a first test problem we considered a long wall of constant thickness loaded uniformly in two directions, as shown in Figure 2. The grid used is shown in the same figure and we took  $C_1 = 80$  psi,  $C_2 = 20$  psi. The computed and the values obtained from the analytic solution of various field variables are shown in Table I. It is obvious that the computed results, without using

equilibrium iterations, agree very well with those obtained from the exact solution. A reason for getting such good numerical results with a rather coarse grid is that the exact solution corresponds to a homogeneous deformation of the wall and this deformation mode is included in the displacement field assumed within an element.

Table I

No. of load inc.	$E_{xx} \dagger$	$E_{yy} \dagger$	$T_{xx} \dagger$ (psi)	$T_{yy} \dagger$ (psi)	$u_x \ddagger$ (in.)	$u_y \ddagger$ (in.)	$p \dagger$ (psi)
10	-0.156	0.221	-48.9	102	-0.170	0.401	-228.0
50	-0.154	0.221	-49.8	100	-0.168	0.402	-228.5
0 (Exact)	-0.154	0.222	-50.0	100	-0.168	0.403	-228.6

† Values at the centre of element No. 2.

‡ Displacement of nodal point No. 6.

As a second test problem we considered a homogeneous thick-wall cylindrical pressure vessel (inner radius  $R_i = 7$  in., outer radius  $R_o = 18.625$  in.,  $C_1 = 80$  psi,  $C_2 = 20$  psi) loaded internally with a pressure  $p_i$ . Since the developed program can handle only zero displacements prescribed along the axes, i.e. cannot handle oblique boundary conditions, we considered a quarter of a circle and divided that into 10 uniformly spaced elements in the radial direction and 20 equally spaced elements across the circumference, as shown in Figure 3. This grid is called a  $10T \times 20C$

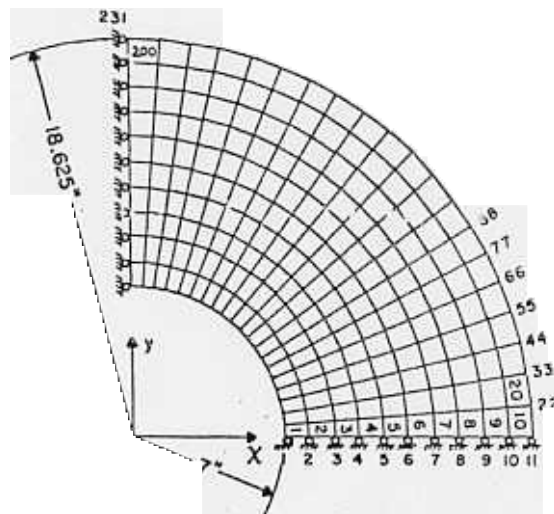


Figure 3. Finite element representation for an infinitely long thick-walled cylinder

grid and should provide a severe test of the finite element formulation since the results should come out to be axisymmetric. This problem with the same geometric and material parameters has been solved by Scharnhorst and Pian<sup>3</sup> by using a mixed model, and by Oden and Key<sup>5</sup> by using an axisymmetric formulation. An exact solution of the problem obtained as a special case

of a problem solved in Section 3.3 of the book by Green and Zerna<sup>8</sup> is

$$\begin{aligned}
 T_{rr} &= p + 2C_2 + 2(C_1 + C_2) \frac{R^2}{r^2}, \\
 T_{\theta\theta} &= p + 2C_2 + 2(C_1 + C_2) \frac{r^2}{R^2}, \\
 p &= -p_i - 2C_2 - 2(C_1 + C_2) \left[ \ln \frac{r}{R_i} + \frac{b}{2} \left( \frac{1}{r^2} - \frac{1}{R_i^2} \right) - \ln \frac{R}{R_i} + \frac{R^2}{r^2} \right], \\
 p_i &= (C_1 + C_2) \left[ \ln \frac{R_i^2 + b}{R_o^2 + b} - 2 \ln \frac{R_i}{R_o} + b \frac{R_o^2 - R_i^2}{(R_o^2 + b)(R_i^2 + b)} \right], \\
 b &= 2R_i \bar{u}_r + \bar{u}_r^2 = 2Ru_r + u_r^2, \\
 r &= R + u_r, \\
 E_{rr} &= \frac{1}{2} \left( \frac{R^2}{r^2} - 1 \right), \quad E_{\theta\theta} = \frac{1}{2} \left( \frac{r^2}{R^2} - 1 \right).
 \end{aligned} \tag{14}$$

In these equations  $u_r$  is the radial component of displacement,  $\bar{u}_r$  is the radial displacement of a point on the inner surface,  $T_{rr}$  is the radial Cauchy stress,  $T_{\theta\theta}$  is the circumferential Cauchy stress,  $R$  is the radius of a point in the undeformed reference configuration,  $E_{rr}$  is the radial strain and  $E_{\theta\theta}$  is the strain in the circumferential direction.

The results obtained from the analytical solution (14) and those computed from the finite element program without using equilibrium iterations are given in Table II. It is clear that the computed values of various field quantities appear to converge to their values obtained analytically. However, the rate of convergence is awfully slow. Even with the entire load divided into 70 equal increments, the computed values differ by about 6 per cent from their values obtained from (14). In order to assess the effect of refinement of the grid we computed results by using a  $20T \times 40C$  grid. There was no noticeable improvement in the results, implying thereby that the  $10T \times 20C$  grid was adequate.

A comparison of these results with those of Scharnhorst and Pian<sup>3</sup> reveals that, without the use of equilibrium iterations, the Reissner-type variational principle yields acceptable results

Table II

No. of load inc.	$u_r, \ddagger$ (in.)	$E_{\theta\theta} \dagger$	$E_{rr} \dagger$	$T_{\theta\theta} \dagger$ (psi)	$T_{rr} \dagger$ (psi)	$p \dagger$ (psi)	% Error† in incompr. constraint
10	5.795	0.997	-0.334	417	-119	-234.7	3.35
20	6.302	1.11	-0.351	460	-126	-232.7	1.94
30	6.527	1.17	-0.354	475	-134	-231.8	1.24
40	6.660	1.20	-0.356	492	-130	-231.4	1.08
50	6.742	1.22	-0.357	500	-131	-231.1	0.90
60	6.803	1.23	-0.358	505	-131	-231.0	0.77
70	6.848	1.24	-0.359	509	-132	-230.8	0.67
Exact	7.182	1.32	-0.363	539	-135	-230.0	0.0

† Values at the centre of element No. 1

‡ Radial displacement of interior node.

Table III

No. of load inc.	$u_r$ ‡ (in.)	$E_{\theta\theta}$ †	$E_{rr}$ †	$T_{\theta\theta}$ † (psi)	$T_{rr}$ † (psi)	$p$ † (psi)	% Error† in incomp. constraint	Tolerance in displacements (%)
30 load inc. with up to 10 eq. iter.	7.136	1.31	-0.367	539	-133	-232.3	1.61	0.1
50 load inc. with up to 15 eq. iter.	7.152	1.317	-0.365	539	-134	-231.4	1.0	0.01
Exact	7.182	1.323	-0.363	539	-135	-230.0	0.0	0.0

† Value at the centre of element No. 1.

‡ Radial displacement of interior node.

with the load divided into fewer increments. For example, with the load divided into 29 steps, the use of mixed model and the stationary potential energy principle give almost identical errors in the values of the hydrostatic pressure and incompressibility constraint at the centre of element No. 1, but the value of radial displacement of the interior node has an error of 1 per cent with the mixed model and an error of 7 per cent with the use of the stationary potential energy principle. As expected, the presently computed values of  $\bar{u}_r$ ,  $E_{rr}$ ,  $E_{\theta\theta}$ ,  $T_{rr}$  and  $T_{\theta\theta}$  converge from below to their values obtained from the analytical solution. Whereas, for  $p_i = 128.2$  psi and the load divided into 40 steps with no equilibrium iterations used, Oden and Key<sup>5</sup> who used an axisymmetric formulation and constant strain triangular elements report an error of 2.4 per cent for the radial displacement, we get an error of 7.4 per cent for  $p_i = 150$  psi and the load divided

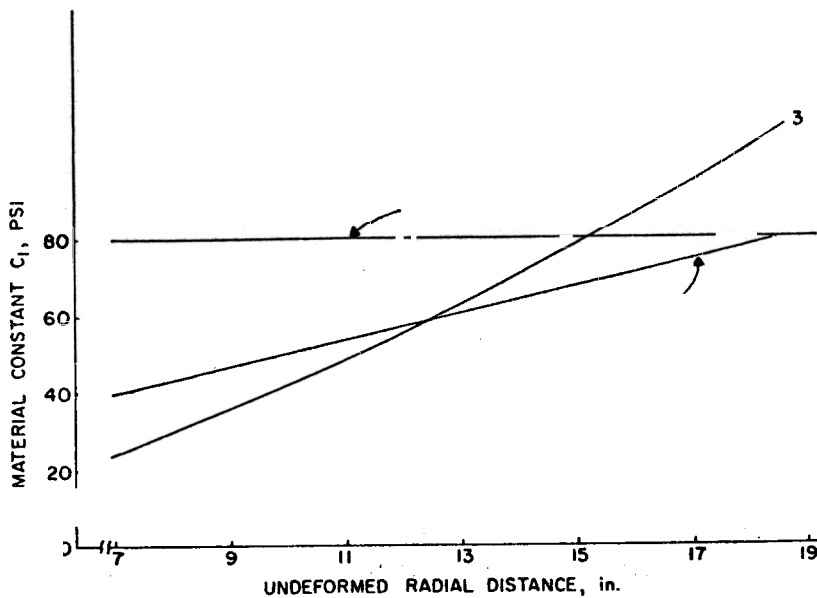


Figure 4. Material constant  $C_1$  vs. the undeformed radius

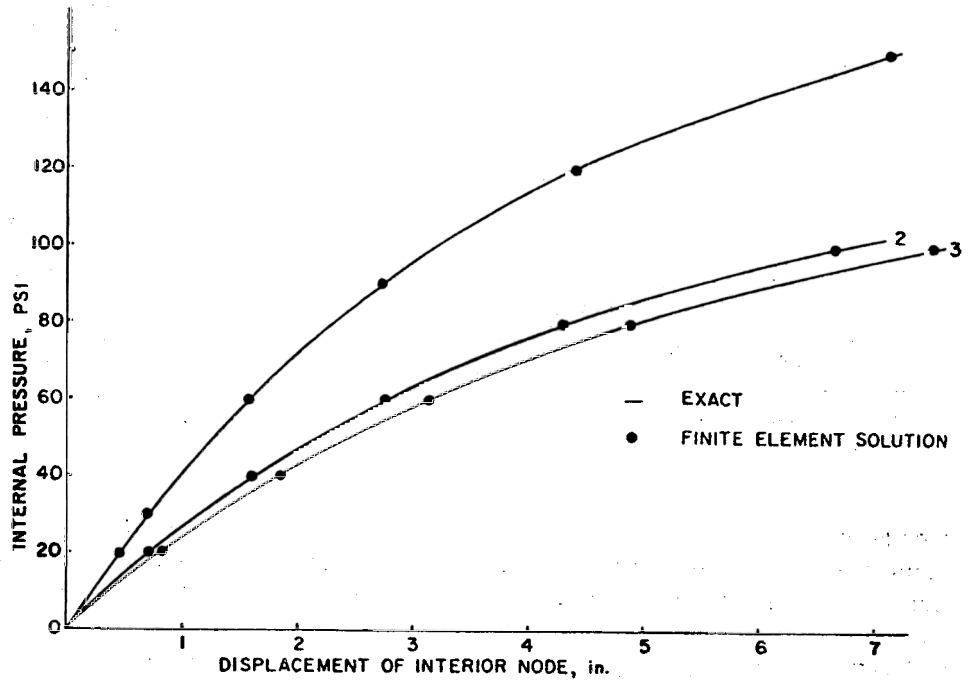


Figure 5. Internal pressure vs. the radial displacement of a point on the inner surface

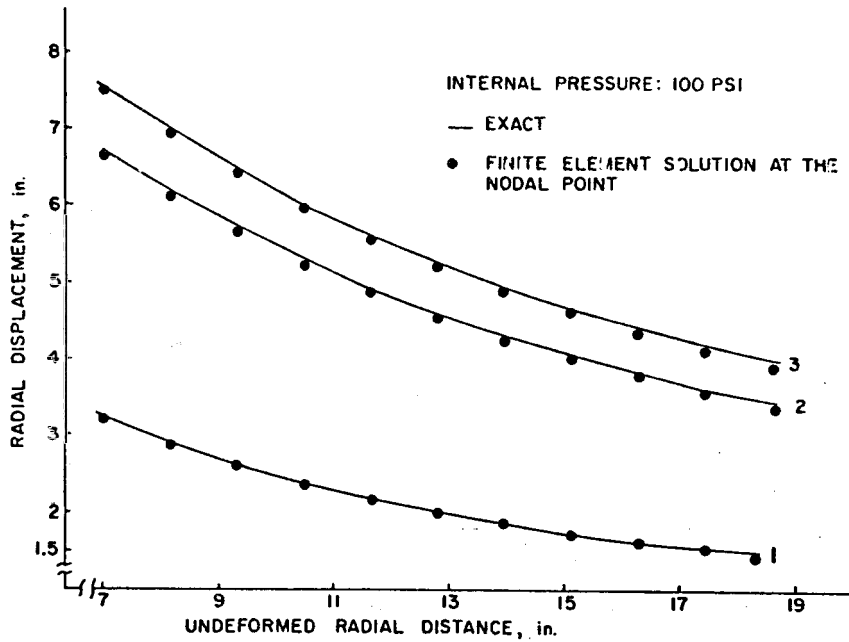


Figure 6. Radial displacement vs. the undeformed radius

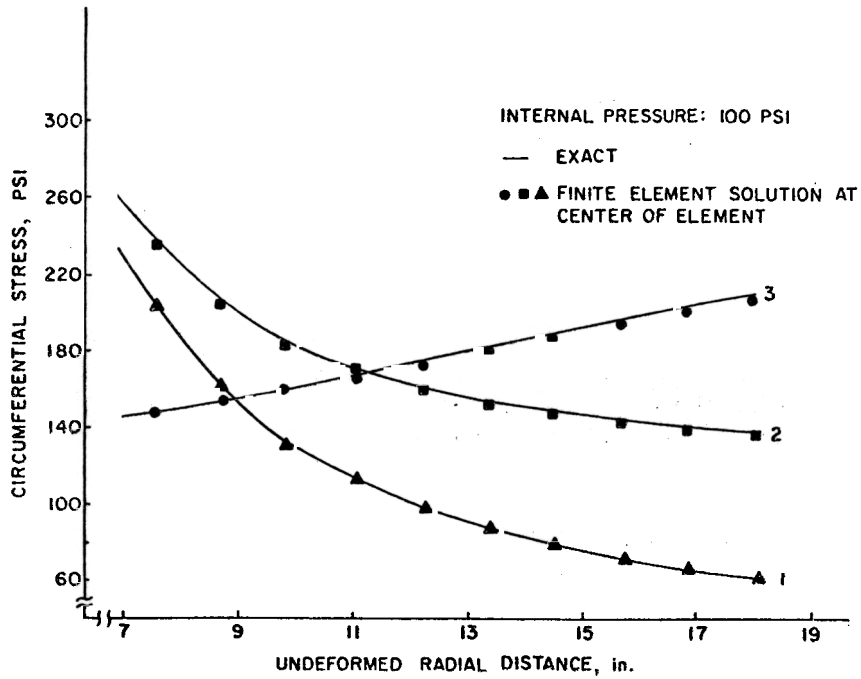


Figure 7. Circumferential Cauchy stress vs. the undeformed radius

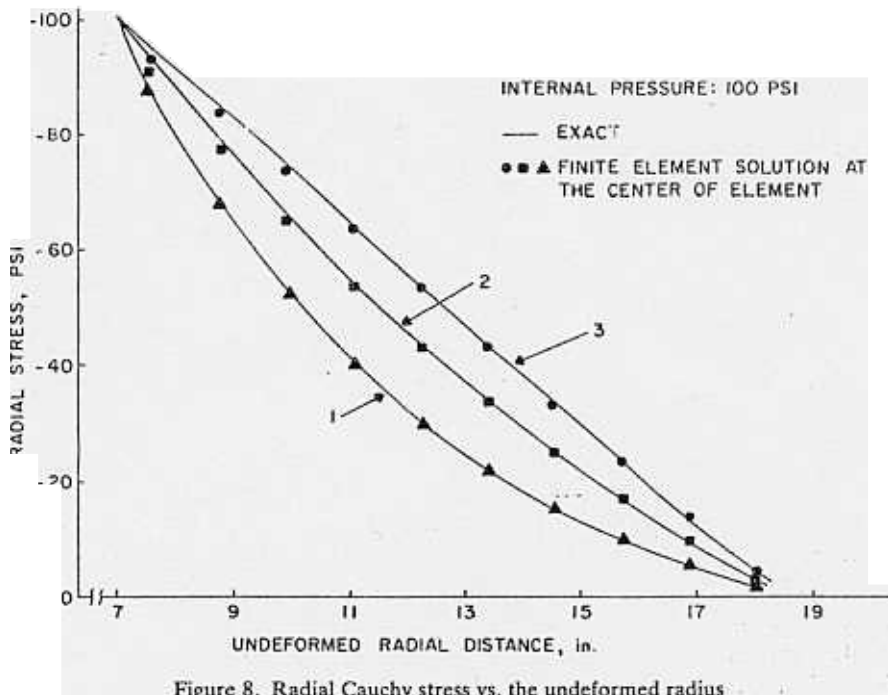


Figure 8. Radial Cauchy stress vs. the undeformed radius

into 40 steps. Therefore, for this problem, axisymmetric formulation and the Reissner-type variational principle give faster convergence if equilibrium iterations are not used.

With the use of equilibrium iterations, as can be seen from the results presented in Table III, the accuracy of the results is significantly improved. When using equilibrium iterations, the iterative process within a load step was stopped when the ratio of the Euclidean norm of the newly computed displacements of the nodal point to the Euclidean norm of the total displacements of the nodal point up to the immediately preceding iteration was less than a pre-specified number. As is clear from the results presented in Table III, with tolerance set equal to 0.001, the computed results agree closely with those obtained from the analytical solution.

We note that the use of equilibrium iterations results in improved numerical results because the pressure load is applied on the deformed shape. Thus, if the displacements are underestimated after any load step, from there on the structure will always be underloaded and the error in the computed displacements will keep on increasing. It seems that if the applied load is a dead loading, then the results obtained should be less sensitive to the use of equilibrium iterations.

In order to assess the effect of the nonhomogeneity of the material on the number of load steps and the number of equilibrium iterations required for the numerical solution to converge to the analytic solution, we also studied the pressure vessel problem for the cases when the material constants  $C_1$  and  $C_2$  are given by

$$C_1 = 15.914 + 3.4409 R \text{ psi}, \quad C_2 = C_{1/4}, \quad (15)$$

$$C_1 = -7.3759 + 3.4409 R + 0.148 R^2 \text{ psi}, \quad C_2 = C_{1/4} \quad (16)$$

We identify the problem of the homogeneous cylinder as problem 1 and the other two problems for which  $C_1$  and  $C_2$  are given by (15) and (16), respectively, as problems 2 and 3. The variation of  $C_1$  with the undeformed radius  $R$  is plotted in Figure 4.

For homogeneous materials, dividing the internal pressure of 150 psi into 30 equal increments and using up to 15 equilibrium iterations gave displacements accurate to within 0.1 per cent of their values. However, for problems 2 and 3, the same accuracy could not be achieved with everything else such as the number of increments into which the load is divided etc. kept the same. Since the computer time for each complete run was approximately 4.5 CPU minutes on an IBM 370/168 computer, it was decided to reduce the tolerance on displacements to 1 per cent of their values. As should be clear from the results presented in Figures 5 to 8, for homogeneous materials, the values of displacement and stresses came out very close to those obtained from the analytical solution. For nonhomogeneous materials of problems 2 and 3, the same accuracy on displacements could not be attained for internal pressure  $p_i$  greater than or equal to 120 psi with the number of increments into which the load is divided and the maximum number of equilibrium iterations kept the same as those for problem 1. Of course, the accuracy can be improved by increasing the number of steps into which the load is divided and/or the number of equilibrium iterations. What this numerical experiment establishes is that for nonhomogeneous materials one will, in general, need to divide the load into more number of increments and/or increase the number of equilibrium iterations to arrive at the same accuracy in displacements. How many more steps into which the load is to be divided or what is the optimum number of equilibrium iterations depends upon the specific problem. It seems rather safe to conclude from the preceding, as turned out to be the case for the results presented herein, that CPU time required to solve a problem when the material is nonhomogeneous is more than that required to solve an identical problem with the material being homogeneous.

Results depicted in Figure 5 show that for the same internal pressure, as expected, points on the inner surface undergo larger radial displacement for problems 2 and 3 as compared to that for problem 1. This is so because the material of problem 2 is softer than that of problem 1. Even though the material of problem 3 is harder than that of problem 1 or 2 near the outer surface and softer near the inner surface, points on the inner surface undergo larger radial displacement for problem 3 than they do for problem 1 or 2. From Figure 6 we see that the difference between the radial displacement of a point for any two of the three problems is more for a point on the inner surface than that for a point on the outer surface. A reason for this is that the material of the cylinder is assumed to be incompressible and, therefore, points on the outer surface ought to undergo less radial displacement in order to keep the area of cross-section unchanged.

In Figure 7 is plotted the variation of circumferential Cauchy stress through the thickness of the cylinder. Since the values of material constants of problem 3 at the outer radius are considerably higher than their values at the inner radius, the outer layers exert significantly higher pressure on the inner layers than they do when the material is homogeneous. Thus in this case the circumferential Cauchy stress increases as we go outwards from the inner radius. This is opposite of what happens for problems 1 and 2. This suggests that by suitably varying the values of material constants through the thickness of the cylinder, one can make the circumferential Cauchy stress to be more or less uniform through the thickness of the cylinder and thereby make optimum use of the material. The variation of the radial Cauchy stress across the thickness of the cylinder is plotted in Figure 8.

Results presented in Figures 5 to 8 attest to the closeness of numerical results to the one obtained from the analytical solution. At the risk of repetition we add that to achieve the same accuracy in displacements one will need, in general, to divide the load into a larger number of increments and/or use more equilibrium iterations for nonhomogeneous materials than for homogeneous materials.

### REMARKS

Equation (14) makes clear that for plane strain deformations of a thick-wall cylindrical pressure vessel, the values of  $T_r$ ,  $T_{\theta\theta}$ ,  $E_r$ ,  $E_{\theta\theta}$  and  $u$ , depend upon the material constants  $C_1$  and  $C_2$  only through their sum ( $C_1 + C_2$ ). The value of hydrostatic pressure  $p$  depends upon  $C_2$  and ( $C_1 + C_2$ ) and therefore  $T_{zz}$ , the normal stress on a cross-section, will depend upon  $C_1$  and  $C_2$ . The preceding result can be proved to be true for general plane strain deformations of homogeneous Mooney–Rivlin materials.

The developed computer program differs from NONSAP in the way the stiffness matrix is assembled and the linear equations are solved. Whereas in NONSAP, the applied loads are dead loads, loads that always act normal and tangential to the deforming surface can be accounted for in this program. In Reference 9, a problem in which the applied load is normal to the deformed surface has been solved by using the present program.

### ACKNOWLEDGEMENT

I am indebted to Dr. Scharnhorst and a referee for their constructive criticisms of two earlier drafts of this paper.

### REFERENCES

1. K. J., Bathe, E. L., Wilson and R. H., Iding, 'NONSAP—a structural analysis program for static and dynamic response of nonlinear systems', *SESM Report No. 74-3*, Department of Civil Engineering, University of California, Berkeley (1974).

2. K. J. Bathe, E. Ramm and E. L. Wilson, 'Finite element formulations for large deformation dynamic analysis', *Int. J. num. Meth. Engng*, **9**, 353-386 (1975).
3. T. Scharnhorst and Theodore H. H. Pian, 'Finite element analysis of rubberlike materials by a mixed model', *Int. J. num. Meth. Engng*, **12**, 665-676 (1978).
4. J. T. Oden, 'Finite plane strain deformations of incompressible elastic solids by the finite element method', *Quart. Aeronautics*, **19**, 254-264 (1968).
5. J. T. Oden and J. E. Key, 'Numerical analysis of finite axisymmetric deformations of incompressible elastic solids of revolution', *Int. J. Solids Structures*, **6**, 497-518 (1970).
6. J. T. Oden, *Finite Elements of Nonlinear Continua*, McGraw-Hill, New York, 1972.
7. L. D. Hofmeister, G. A. Greenbaum and D. A. Evensen, 'Large strain, elasto-plastic finite element analysis', *AIAA J*, **9**, 1248-1254 (1971).
8. A. E. Green and W. Zerna, *Theoretical Elasticity*, 2nd edn, Oxford University Press, London, 1968.
9. R. C. Batra, 'Rubber covered rolls, the nonlinear elastic problem', Presented at *2nd Int. Conf. on Computational Methods in Nonlinear Mechanics*, University of Texas at Austin, TX (1979). *J. Appl. Mech.* (in press).